As originally published in the SMTA Proceedings.

Comparison of Component Assembly Process-Reliability Relationships of Low-Temperature Solders and ECAs on Flexible Direct-Write Additive Circuits

Pradeep Lall, Jinesh Narangaparambil
Auburn University
NSF-CAVE3 Electronics Research Center
Department of Mechanical Engineering
Auburn, AL 36849, USA
E-mail: lall@auburn.edu
Tele: +1(334)844-3424

Scott Miller
NextFlex Manufacturing Institute
San Jose, CA 95131

ABSTRACT
Fabrication of additively printed flexible hybrid circuits requires the development of component attachment methods with low-temperature processing. Some substrate materials, including thermally stabilized PET and PEN require a peak processing temperature of less than 150°C. Several new low-temperature solder materials have emerged capable of being processed at temperatures in the range of 130-150°C to access the benefits of lower warpage, lower energy consumption, and lower carbon footprint. This paper studies the process-performance-reliability relationships for Sn-Bi-Ag and Sn-In solders on additively printed copper metallization. Process recipes have been developed for direct write additive printers to fabricate single-layer and flexible multilayer circuits. Copper ink is a good and cost-effective alternative to silver ink, but its use has lagged due to an increased propensity for oxidation during manufacturing. In this paper, photonic curing has been used to sinter copper ink to make the traces conductive. The method flashes high-energy light that sinter metal particles instantaneously, and the temperature of the substrate remains low. The effect of the different photonic sintering profiles on the mechanical and electrical properties of the printed traces has been studied. Electrical and mechanical performance has been studied through the characterization of the frequency performance of low-pass filters, high-pass filters, and amplifiers fabricated using surface mount components on additively printed metallization. Reliability and the performance degradation of the additively printed circuits have been quantified in flex-to-install applications. In addition, SEM/EDAX has been used to study the intermetallics at the interface of LTS and additively printed circuits.
Keywords: Direct-Write technique, Additive printing, Flexible electronics, Copper ink, Electrically Conductive Adhesive, Low-Temperature Solder, Reflow.

INTRODUCTION

Demand for the development of flexible-hybrid electronics manufacturing methods has been pushed by product developments that involve closer integration of electronics into the intended application. The emergence of thin, flexible form-factors for electronics product design is a byproduct of the miniaturization of electronics. Traditional electronics frequently employ rigid printed circuit boards, which restricts the level of integration that may be achieved and the packaging required for dependable performance in the final application. Through techniques for creating non-planar electronic designs, the development of additive print processes offers opportunities for closer integration of form and function. Additionally, using additive techniques eliminates the mask and etch processes employed in stiff electronics manufacture using subtractive processing. Furthermore, additive printing allows for fewer production operations owing to fewer process steps and cost savings due to lower material usage [1], [2]. Less material consumption equals less environmental effect. Lower temperature processing of printable materials makes it possible to employ flexible substrates like low-cost plastic films.

Low-temperature films' viability requires using low-temperature attachment methods for component assembly. Lower processing temperatures have other benefits, including lower warpage, lower energy consumption during manufacturing and assembly, and a lower carbon footprint. Low-temperature connectivity technologies for flat-panel displays, organic electronics, and low-cost disposable microelectronic devices on plastic substrates are gaining popularity [3]. These substrates, such as PET, polyimide, and paper, as well as some electronic components based on organic groups or nanosized building blocks, are unable to maintain their functions and stabilities at temperatures ranging higher than 200°C, which is required for melting conventional SnAgCu lead-free solders widely used in microelectronics soldering and reflow [4]-[6]. Thus, an enhanced interconnection method that allows for low-temperature processing while withstanding a greater operating temperature is desired.

For a significant period of electronics development, the interconnection of components was dominated by the use of SnPb solders, which required higher processing temperatures greater than 200°C. The transition of electronics away from leaded solders resulted in the emergence of SnAgCu-based solders, which also required higher temperature processing. More recently, several low-temperature interconnection

methods have emerged. Electrically conductive adhesive (ECA) has emerged as a lead-free solder alternative in liquid crystal display (LCD), smart card, flip-chip assembly, chip-scale package (CSP), and ball grid array (BGA) applications [7]-[8]. ECA is a class of materials comprised of fillers (whiskers, platelets, or particles) mixed in polymers (epoxy, silicone, or polyimide) that can provide binding strength and electrical conductivity between substrates and chips. One of the primary benefits highlighted in ECAs is their low processing temperature compared to conventional solders. Similarly, LTS paste processing allows for lower reflow temperatures, cutting energy usage during SMT by up to 40 percent. In order to satisfy the product objectives and maintain high system assembly yields at lower prices, compact and complex systems necessitate an evolution in both SMT methods and materials [9].

This study focuses on performance interaction with different interconnection methods, including electrically conductive adhesive (ECA) and low-temperature solder (LTS). Interconnection materials have been printed using the direct-write method to attach components such as resistors, inductors, capacitors, and LEDs to additively printed circuits. Components have been measured before and after attachment to examine interconnection performance. In addition, the cross-sectional area for the intermetallic formation was examined. The Shear Test (Mechanical Property) of the attached components has also been tested for various applications. OrCAD software has been used to construct and evaluate an inverting Op-Amp circuit. The performance of the inverting Op-Amp circuit has been compared for the interconnection materials used.

PRINT-PLATFORM AND INKS

For the printing, the direct-write technique was used on the nSrypt Printer. Inks have been dispensed during the print process using Smart Pumps on the direct-write platform. A Luer adapter nozzle has been used for the print process. Figure 1 shows the direct write setup used to print conductive and binding material.

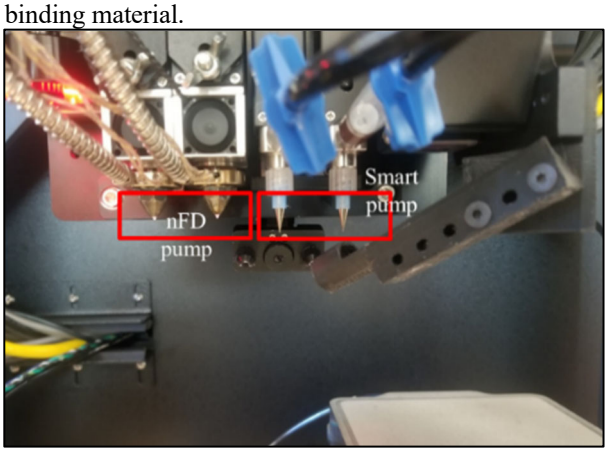

Figure 1: nFD and Smart pump set up on the system

A. Cu-Ink Description

Test vehicle circuits were additively printed using a copper paste that can be processed post-print using laser and photonic sintering. By adjusting the burst energies, photonic sintering enables the processing of the printed metallization at lower temperatures. In addition, compared to silver inks, copper enables fabrication utilizing less expensive inks to construct circuits. Prior to being loaded onto the direct-write print platform, the inks were blended in a planetary mixer. Table I shows the ink properties of the conductive paste used in this paper. Copper ink has a high solid concentration of 82 percent and a viscosity of 25,000–30,000 cps.

Table I: Conductive Ink Properties

Parameters	Value
Description	Cu ink
Viscosity	25,000-30,000cP at 50sec^{-1}
Solid content	82 wt%
Sheet resistivity	10mΩ/sq/mil

B. Electrically Conductive Adhesive (ECA) paste

The authors' earlier research with the ECA has determined that 150°C for 30 minutes is the ideal curing temperature for the silver-based ECA ink [10]. Conducive inks made of copper or silver can be used with the ECA. Table II shows the ink properties of the ECA paste used in this paper. The ECA used in the study is thixotropic with a viscosity of 110,000 cP at a shear rate of 1 sec^{-1} and a viscosity of 15,000 cP for a shear rate of 100 sec^{-1}.

Table II: ECA Ink Properties

Parameters	Value
Viscosity	110,000cP at 1 sec^{-1} 30,000cP at 10 sec^{-1} 15,000cP at 100 sec^{-1}
Specific gravity	3.2
T_g	-10˚C
Volume Resistivity	< 9 x 10^5 Ω*cm

C. Low-Temperature Solder (LTS) Paste LTS1 - SnBiAg

LTS1 is a SnBiAg halogen-free, air-reflow capable, no-clean solder paste. The paste has good wetting capabilities and is designed to leave a moderate residue. The solder paste can be used in low-temperature connectivity with a lead-free solution thanks to its low-temperature activation. The material composition is shown in Table III. Progressive heating, followed by a cool-down profile, is used for processing. A ramp rate of 0.5-1°C/sec is used during the preheat portion of the reflow profile. The melting point of the SnBiAg is 140°C.

Table III: SnBiAg LTS1 Ink properties

Parameters	Value
Material Composition	57Bi/42Sn/1Ag
Heating Ramp Rate	0.5-1˚C/second
Melting Point	140˚C

D. Low-Temperature Solder (LTS) Paste LTS2 - SnIn

LTS2 is a no-clean, halide-free SnIn solder paste. Reduced metallization of precious metals like gold or silver leaching/scavenging and better ductility to compensate for thermal expansion coefficient (CTE) differences between different materials are two advantages of indium-containing alloys. LTS2 is an air-reflow paste with a medium residue and good wetting properties. The material composition is shown in Table IV. A ramp rate of 0.5-1°C/sec is used during the preheat portion of the reflow profile. The melting point of the SnBiAg is 150°C.

Table IV: SnIn LTS2 Ink properties

Parameters	Value
Material Composition	52Sn/48In
Heating Ramp Rate	0.5-1˚C/second
Melting Point	150˚C

TEST VEHICLE DESIGN

Test vehicles were developed and fabricated at the CAVE3 Electronics Research Center. Polyimide flexible substrate is used for printing processing and component assembly to fabricate the test vehicle. The polyimide substrate is 5 mils thick and has been plasma-cleaned at 100W for 5-minutes with oxygen. The polyimide material can withstand temperatures of up to 300°C.

A. Test Vehicle Design – 1

The test vehicle was created to investigate the sintering profile and print process. Five lines represent each condition with pads at either end. In order to guarantee that the printing is consistent for a certain process parameter, the number of traces is set to 5. Each test condition is repeated three times to evaluate the variation in the print output.

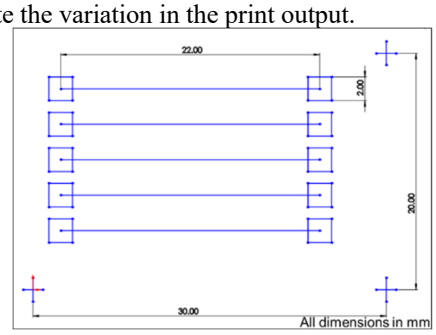

Figure 2: Test vehicle design 1

Table V: Various sintering conditions

Parameters	Variation
Sintering conditions	• Energy • Frequency • Stage speed of the photonic system

Figure 2 shows this paper's test vehicle used for the sintering study. For high print quality, Cu ink has been tested for different process factors, including printing speed and ink pressure. Consistent ink deposition with a precise trace definition is a desirable print characteristic. Mechanical and electrical characteristics have been investigated with respect to the changing process parameters and their impact on the print profile including trace height and trace-width. The mechanical and electrical properties have been assessed with the changes in the cross-section area. Based on prior research by authors presented in [11], [13], the print process has been optimized to print at a print-speed of 3mm/s at 15psi ink-pressure. Voltage is used to define the maximum and peak energy for photonic curing. The total energy is controlled through the specification of on-time and off-time in the burst sequence. The photonic curing process can be run in several modes, including single-pulse, burst mode, which involves a specified duration pulse sequence, and continuous mode. In addition, the curing profile can be controlled through the specification of the stage speed during pulse-flash, step-size, which defines the forward movement and flash energy overlap. In the prior work, the authors have also shown the influence of the sintering profile on the realized electrical and mechanical performance [13]. The effect of downstream thermal processes during component assembly on the prior realized print-properties is studied.

B. Test Vehicle Design – 2

The purpose of test design-2 is to establish the interconnection between discrete components and printed conductive traces to check the functionality of the ECA and LTS materials. The process-flow for attaching the components is shown in Figure 3. Before being attached to the stage, the polyimide substrate used in this study was plasma cleaned.

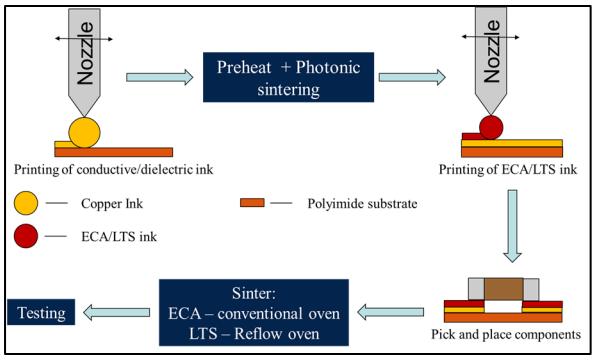

Figure 3: Process Flow for Component Attachment Using LTS Paste

This design is used to compare measured values to rated values of commonly available components, including resistors (R), capacitors (C), inductors (L), and LEDs. The first layer of conductive ink (Layer 1) is printed and then cured. After heat treatment, the sample is transferred to the stage, and fiducial matching is followed by interconnection paste printing (Layer 2). The components are pick-n-placed on the printed pads on the interconnection material, followed by sinter or reflow in the oven for ECA and LTS, respectively.

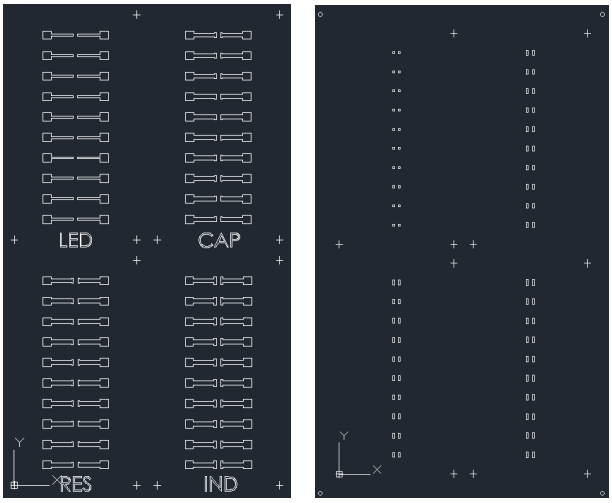

(a) (b)

Figure 4: Design for Test Vehicle Design-2 (a) Layer 1 (b) Layer 2

Layer 1 is illustrated in Figure 4(a) has been printed with a standoff height of 50µm for the conductive traces. Layer 2 in (b) is printed at a 100µm standoff height from the polyimide surface. The standoff height has been raised to account for the trace height from Layer 1. Table VI describes the components used in the test vehicle–2.

Table VI: Specification Of the Discrete Components

Component	Code	Rated value	Dimension (L x W x H), mm
Resistor	0805	1kOhms	2.00 x 1.25 x 0.60
Capacitor	0805	1.8pF @ 7.96 MHz	2.00 x 1.25 x 0.70
Inductor	0806	2.2uH @ 1 kHz	2.00 x 1.25 x 1.80
LED		1.8V	9.27 x 7.87 x 1.10

C. Test vehicle Design – 3

Test vehicle-3 is the Inverting Amplifier Op-Amp circuit has been designed to serve as a device demo based on the study performed with test vehicles – 1 and 2. The op-amp circuit has been designed and analyzed for working in the Or-CAD software, which will be used for comparison with the printed test circuits.

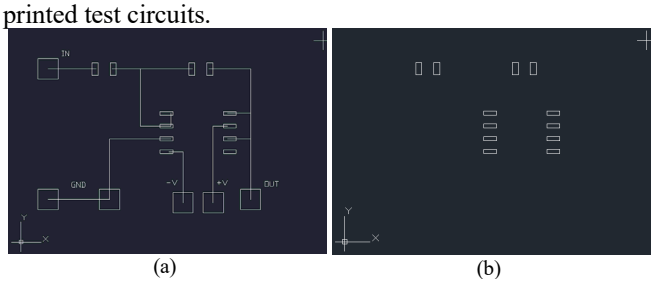

(a) (b)

Figure 5: Design for Test Vehicle Design-2 (a) Layer 1 (b) Layer 2

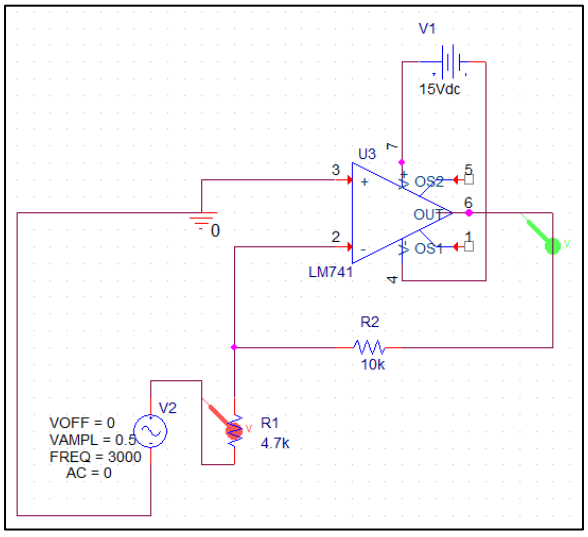

Figure 6: Inverting Op-Amp circuitry from Or-CAD

Figure 5 shows the print design for the inverting circuitry. Layer 1 is conductive ink printing, whereas layer 2 is for binding material printing. The pad sizes printed for the ECA and LTS are based on the component data sheet design for the solder pads. The simulation performance of the inverting circuit is compared with the actual output of the printed flexible circuit. Figure 6 shows the schematic diagram for the amplified inverting op-amp circuitry. The circuitry is designed for an amplification factor of 2.13. The circuit includes two resistors each of 10kohms and 4.7kohms with a generic op-amp. The circuit is powered with a ±15V DC supply.

REFLOW PROFILES FOR LTS

The influence of sintering/reflow required for ECA processing and LTS processing has been studied to understand the effect of the downstream assembly steps on the prior realized performance of the additively printed circuits. The ECA has been sintered at 150°C for 30-minutes. Figure 7 shows the reflow profile for LTS1 (SnBiAg). A peak temperature of 25–45°C (175°C shown) above the melting point of the solder alloy is needed to form a quality solder joint and achieve acceptable wetting and formation of intermetallic layer. Figure 8 shows the reflow profile for LTS2 (SnIn). A peak temperature of 25–45°C (215°C indicated) over the melting point of the solder alloy is required to establish a quality solder junction and ensure adequate wetting owing to the creation of an intermetallic layer.

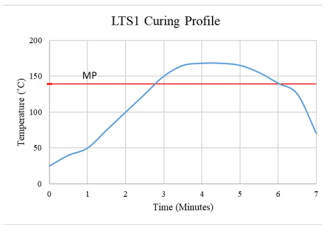

Figure 7: Reflow Profile for LTS1 SnBiAg Paste

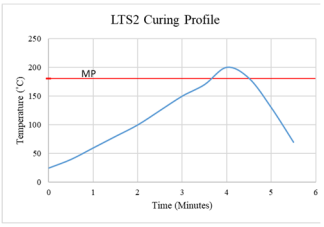

Figure 8: Reflow Profile for LTS2 SnIn Paste

FLEX TO INSTALL TEST SET-UP

The samples are tested in their fold condition on a 25mm and 50mm diameter curved surface. For flex-to-install test configuration, the test design-2 with assembled light emitting diodes assembled on additively printed metallization is mounted on the curved cylinders. The LED attached using three interconnection materials has been compared for performance in the flat-state vs flex-to-install.

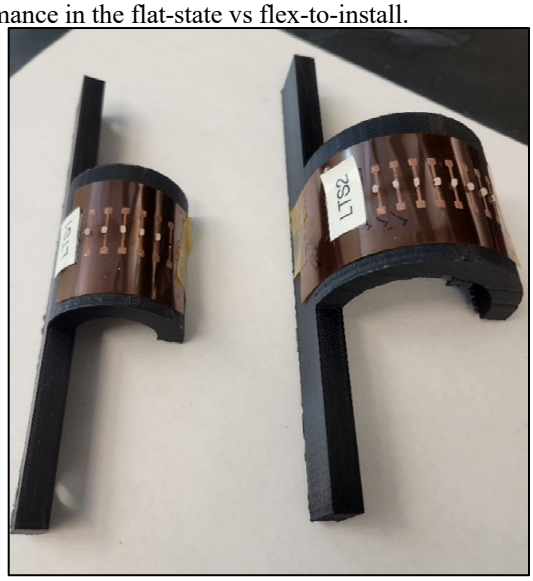

Figure 9: Folding reliability test setup

The curve fixtures used for the folding test reliability are depicted in Figure 9. The LEDs are powered while folded to test their connection under various folding diameters. It is critical to test its mechanical strength and the components' ability to work under tight bends.

EFFECT OF PHOTONIC SINTERING CONDITIONS

In photonic sintering, several factors must be addressed including voltage, on-time, off-time, burst mode, stage speed and step size. Each parameter modification defines the quantity of cure. The system's aperture size is set at 80mm, the maximum slit size maintained throughout the study in this paper. In this experimental leg, the photonic sintering process evolution with increased temperature exposure due to the component attachment with varied sintering parameters is studied.

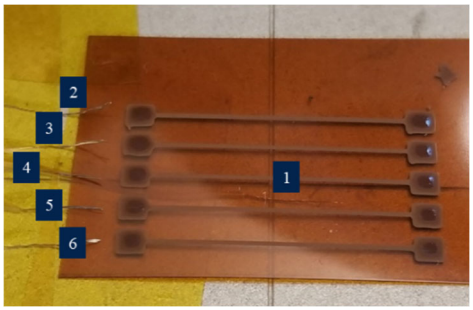

Figure 10: Thermocouple numbering for temperature measurement during light flashing

Thermocouples have been installed in the vicinity of the printed circuits to assess the temperature during the photonic sintering profile. Figure 10 shows the positioning of thermocouples on the sample at each trace to measure the exposed temperature under different curing conditions. The thermocouple labeled "1" is located beneath the polyimide substrate, while the remaining thermocouples are on the substrate's upper surface. The temperature given in this section is the mean of the highest temperature readings observed. The thermocouples continuously collect data throughout the flash.

A. Effect of Pre-heat

The effect of preheating the traces after printing in a conventional oven for a brief time to dry up the ink before photonic sintering has been explored in order to avoid trace degradation. Samples sintered without preheating experienced popcorn failure at various sintering parameters, as reported prior work by the authors[13].

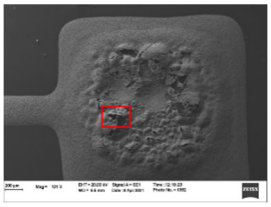

Figure 11: SEM of trace popcorn failure without preheating.

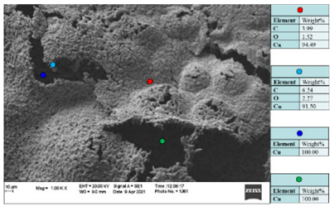

Figure 12: EDX Analysis of one of the photonic cured samples without preheat

The trace composition with and without preheat has been measured using EDX. The samples were subsequently examined for the oxidation trace in both the with and without preheat samples. The following profile was used to cure the samples for this investigation: (a) Voltage = 2000V (b) Energy = 1000 J (c) Frequency = 0.7 Hz (d) Burst Mode – 5 bursts. Figure 11 shows an SEM image of a sample without preheating at the most deteriorated pad location. A circuit's degradation would result in circuit failure and unreliable operation. Figure 12 shows an EDX analysis of a section of the area denoted by the red-boxed region in Figure 11. Different locations have been identified, and their related element compositions have been reported using various color notations. Even though the samples were photonically cured immediately after additive printing of copper, the traces oxidized on the surface, indicating the necessity for an additional step for sintering copper. The green and dark blue points extract data from the lowermost copper layer of the substrate, indicating a 100 percent copper element.

Figure 13 depicts the sintering process, which includes a preheat step to aid in the evaporation of the solvent for proper photonic sintering of the printed conductive metal. The approach also aids in reducing the chances of copper oxidation during sintering.

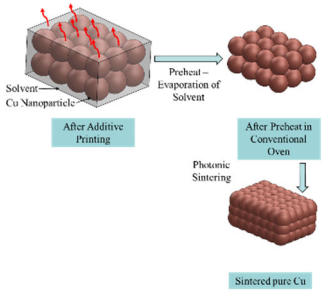

Figure 13: Sintering process flow with preheat

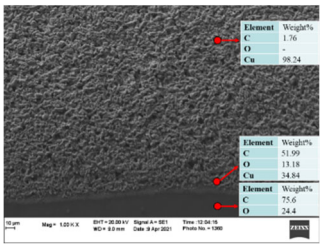

Figure 14: EDX Analysis after preheating at 50C for 15minutes

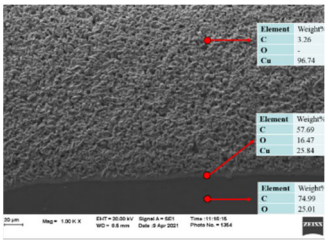

Figure 15: EDX Analysis after preheating at 60C for 15minutes

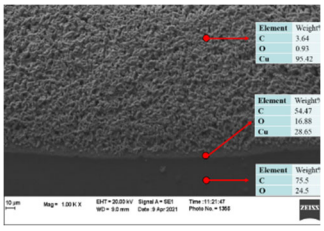

Figure 16: EDX Analysis of one of the samples after preheating at 80C for 15minutes

Figure 14 - Figure 16 shows the EDX analysis of printed copper traces at various preheat temperatures. The information reported in the EDX research is based on an average of three samples. It can be noticed that samples cured after preheating at 50°C and 60°C have no trace of oxygen element, but samples cured after preheating at 80°C have oxygen traces. The popcorn type failure in the samples without preheating is due to the fast-transient heating in photonic sintering and the limited time available for the solvents to evaporate, resulting in deterioration. Preheat is shown to be an effective strategy for avoiding popcorning failures in printed metallization.

B. Effect of Flash Frequency

The flash frequency plays an important role when sintering bigger-sized samples. The parameters that were set

constant for this test are: (a) Voltage = 2000V (b) Energy = 1000J (c) Stage motion: Continuous mode – 2mm/s. The aperture size of the system is set to 80mm, which is the maximum mechanical aperture spacing. Increasing the frequency results in a shorter period, which allows the same amount of energy to be dissipated in a shorter amount of time. The quantity of cure should be more at a higher frequency since the energy flashes at a faster rate, which may help in the agglomeration of the conductive particles. The lowest and maximum frequencies for the stated total energy are 0.1 Hz and 0.7 Hz, respectively.

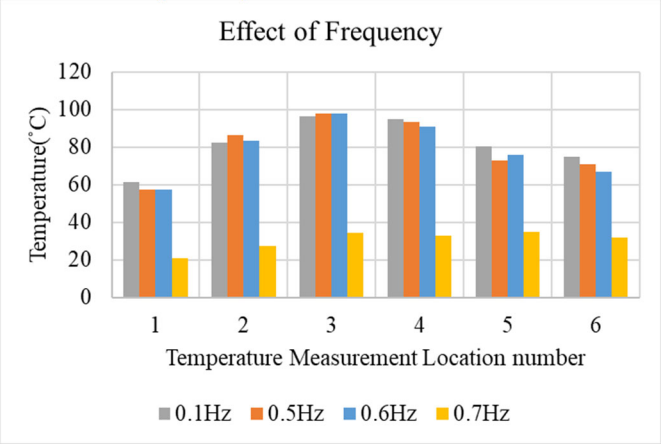

Figure 17: Temperature of the surface at various flash-frequency

Figure 17 shows the impact of varying frequency on the temperature dissipated on the substrate or trace during the sintering process. The 0.7Hz frequency provides far better uniform sintering throughout the processed sample population. Sample populaitons are thus subjected to similar temperatures, which is beneficial for bigger lot sizes or in a continuous industrial operation.

C. *Effect of Flash energy*

The traces were printed with one pass and then sintered with varying flash energy. For this particular testing the following parameters were set as constant: (a) Voltage = 2000V (b) Frequency = 0.7 Hz.

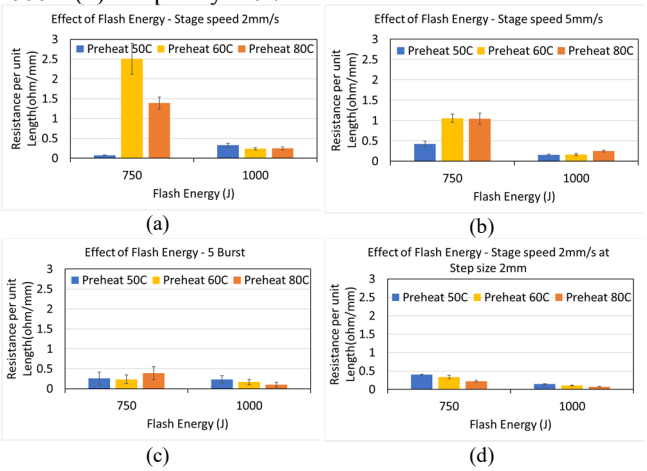

Figure 18: Electrical performance vs flash energy at various stage motions

Figure 18 depicts a comparison of electrical performance for various flash energies. It also covers the influence of various stage motions, which influence the overlap of the flash on the substrate. The test results demonstrate that the step motion stage speed gives an outstanding electrical performance with the lowest resistance per unit length when preheated at 60°C and 80°C with 1000J of flash energy. Figure 19 shows that the shear load to failure values differ extensively over the chosen flash energy and preheat conditions. It can be seen that the flash energy condition with 750J and 60°C preheat has greater mechanical strength in the stage motion depicted in Figure 19b and Figure 19d.

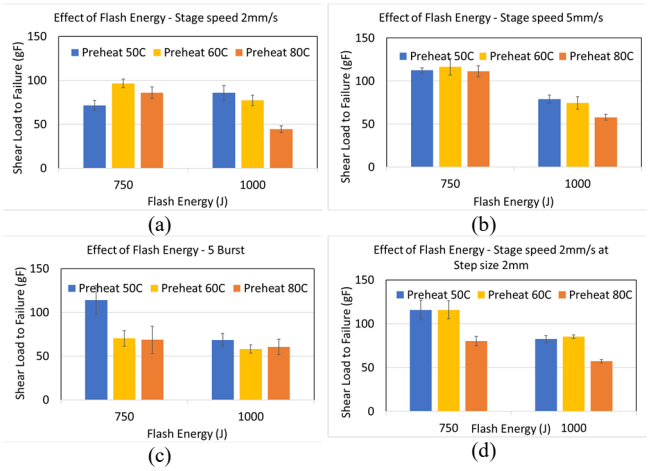

Figure 19: Mechanical performance vs flash energy at various stage motion

D. *Effect of Varying Stage speed*

Sintering conditions should be studied using larger samples to be appropriate for mass manufacturing and larger circuit designs. With varied speed and constant frequency, the proportion of overlap would change, affecting the amount of energy focused at a certain place on the test vehicle. With increasing speed, the overlap percentage decreases, so the degree of cure changes, making it critical to analyze this process. Figure 20 directly compares the printed traces at different stage motions. The resistance per unit length is consistently lower in the samples sintered at 1000J and ran at a stage speed of 2mm/s and a step size of 2mm under all preheat conditions. Figure 21 illustrates a parallel comparison of the printed traces at different stage motions. For all preheat parameters, the shear load to failure value of samples sintered at 750 J is greater than that of samples sintered at 1000J. The samples sintered at 750J with a 60°C preheat run at a stage speed of 2mm/s and a step size of 2mm have the highest mechanical strength of all investigated conditions. In order to examine the physics of the sintering process and how it compares to standard sintering parameters, it was critical to determine the temperature at which the traces are exposed for each stage motion change. For this test, the parameters that were kept constant were as follows:: (a) Voltage = 2000V; (b) Energy = 1000J; (c) Frequency = 0.7 Hz.

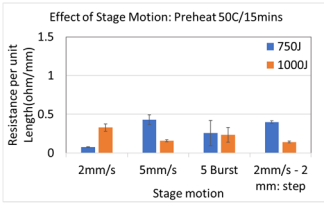

(a)

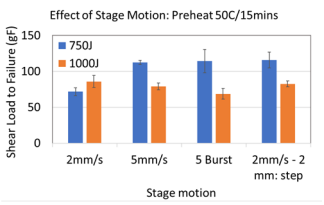

(a)

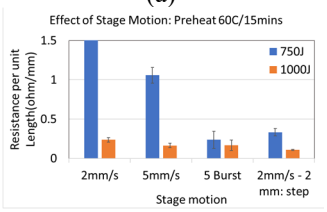

(b)

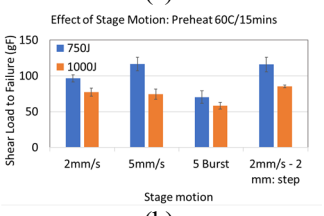

(b)

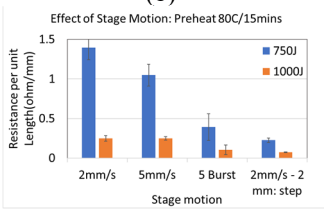

(c)

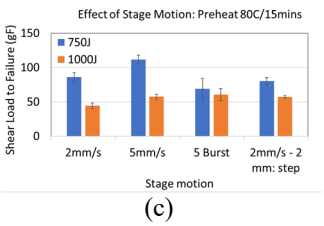

(c)

Figure 20: Electrical performance comparison for various Stage motions

Figure 21: Mechanical performance comparison for various stage motions

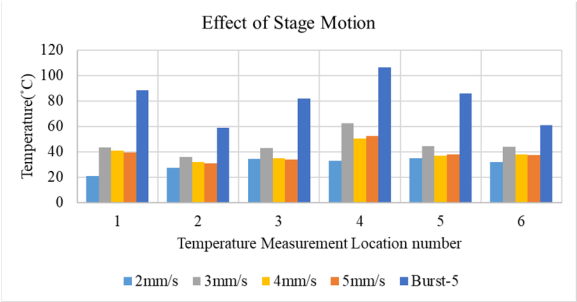

Figure 22: Temperature of the surface vs Stage speed

The temperature measured when the test vehicle is cured under defined conditions with different stage speeds and flash mode is depicted in Figure 22. It was crucial to distinguish between continuous and burst modes. As expected, the burst mode dissipated more heat at the center trace, or where thermocouple number 4 is positioned. The light's concentration was highest in the center and gradually dropped as it travelled away from it. The flash intensity overlap varies in continuous mode depending on the frequency of the flashlight and the stage speed combination, resulting in various sweep patterns. When all conditions are considered, it is clear that the condition with a stage speed of 2mm/s and a frequency of 0.7 Hz has uniform temperature distribution across the test vehicle, providing further confirmation that the combination is the best for the set flashlight parameters for uniform sintering.

E. Effect of Additional Temperature exposure due to interconnect sintering profile

The component attachment procedure comprises extra sintering for the ECA or reflow for the solder, exposing the conducting material to more temperature exposure. It is critical to examine the effect of this additional temperature exposure since over cure of the traces may result in the formation of cracks or deterioration of the traces, resulting in poor mechanical and electrical performance on component attachment. Figure 23 depicts a comparison of the electrical performance of printed copper traces. The results reflect a comparison of the electrical measurements of the traces with sintering conditions without the temperature profile for ECA/LTS indicated "before" and with additional temperature consideration designated as "after" for the conditions described previously. The data is extremely important in determining the photonic sintering profile to utilize for various binding materials. Samples for ECA, LTS1, and LTS2 would have the lowest resistance per unit length if sintered at 2mm/s at 750J flash energy. 1000J provides a stronger cure and might be utilized in regions with only printed traces and no components attachment or multilayer. Figure 24 depicts a comparison of mechanical performance for printed traces before and after additional temperature conditions. The optimal mechanical strength performance result changes depending on the condition and may be studied based on the final application. Samples sintered at 2mm/s at 750J or 1000J are the average performance case scenario.

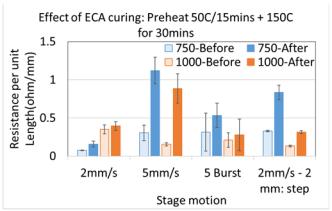

(a)

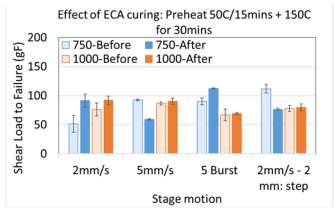

(a)

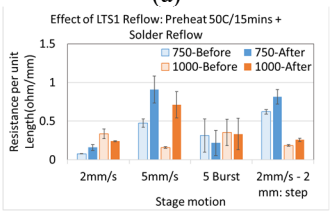

(b)

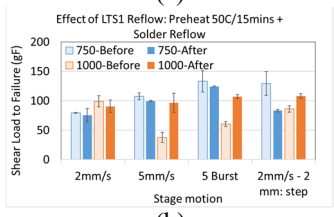

(b)

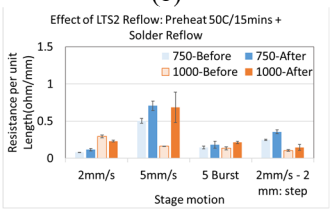

(c)

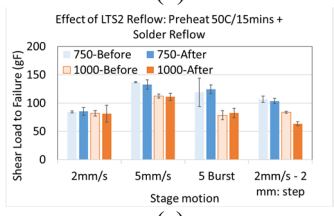

(c)

Figure 23: Electrical performance comparison of additional temperature exposure at a preheat of 50°C for ECA, LTS1 (SnBiAg), LTS2 (SnIn)

Figure 24: Mechanical performance comparison of additional temperature exposure at a preheat of 50°C for ECA, LTS1 (SnBiAg), LTS2 (SnIn)

RLC COMPONENT PERFORMANCE

The test vehicle-1 test findings serve as the foundation for the printing and sintering parameters. The print parameters are completed by taking into account the influence of print speed and ink pressure on the trace profile, which is then related to mechanical and electrical characteristics.

(a) (b) (c)

Figure 25: Image of the trace (a) After sintering the Layer1 (b) After the ECA printing before sintering (c) After the component attachment and sintering

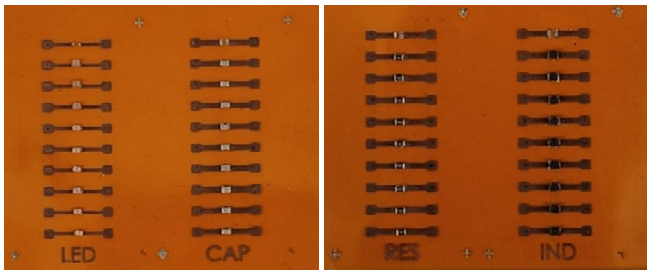

Figure 26: Components attached and notations mentioning each position

Conductive Ink Print process parameters include – (a) Ink Pressure – 15psi (b) Standoff Height – 0.050mm (c) Print speed – 3mm/s (d) Infill Density – 100%. The cure condition for the conductive ink is – (a) Pre heat: 60C for 15mins (b) Photonic sintering conditions include – (i) Voltage = 2000V (ii) Energy = 1000 J (iii) Frequency = 0.7 Hz (iv) Step mode = 2mm/s with step size of 2mm (v) Flash Height = 25.4mm (vi) Mechanical Aperture spacing = 80mm. Figure 25 - Figure 26, depict the component attachment procedure in a step-by-step manner. Copper printing is followed by ECA printing and component attachment, with each layer having its sintering conditions. The amount of binding substance applied has a large impact on the component attachment process as well.

A. Attachment Using ECA Interconnection

The measurements were taken with an Agilent 4192A LF impedance analyzer, as illustrated in Figure 27 - Figure 29. The modules were tested at various frequencies to see how frequency affected interconnectivity. The calculated values fall within an acceptable range. Based on the data and correlation of electrical and mechanical properties stated above, it is reasonable to conclude that ECA interconnection has good characteristics. It can be seen that the post-attachment value with ECA is somewhat higher than the separate components tested before attachment. One explanation for the higher value is that printed copper has a higher resistivity than bulk copper, which contributes considerably to the measurement, and ECA may also offer some resistance. Figure 31 depicts a shear test performed on one of the resistors. Understanding the mechanical strength of a component is significant because it may be utilized for failure analysis of a component in a flexible circuitry during bending, flexing, or twisting. It is also critical to shear the components based on their overall height since this influences the shear strength of the component connection [12]. For the shear test the parameters include (a) Shear height = 20% of the component height from surface (b) Shear tip size =0.60mm (c) Test speed = 12.7µm/s. Shear test results for various components are shown in Figure 30. The shear strength of the components bonded using bonding material was calculated based on their heights. The test height is determined by the component height, which eliminates the application of uneven shear forces. According to the data shown above, the components with lower heights have higher mechanical strength.

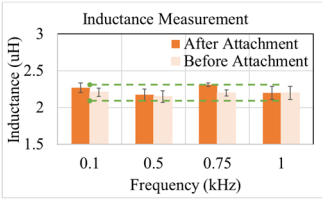

Figure 27: Measurement of the inductor at various frequencies in comparison to rated value

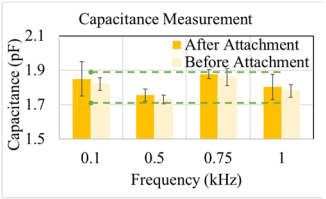

Figure 28: Measurement of the capacitor at various frequencies in comparison to rated value

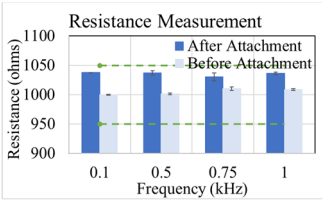

Figure 29: Measurement of the resistor at various frequencies in comparison to the rated value

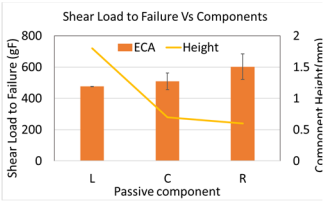

Figure 30: Effect of various component height attachment with ECA on Shear Load to Failure value

Figure 31: Image of one of the samples during shear test

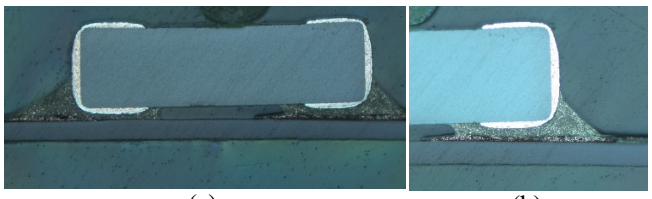

(a) (b)

Figure 32: Cross-sectional optical image component attached using ECA

Figure 32 shows the optical image of the component attached with ECA. The cross-sectional picture depicts the copper and ECA bond, with the copper trace thickness consistent with length, and also demonstrates that the material has been properly sintered. Figure 32 also shows that the bonding substance has created a suitable fillet, suggesting acceptable wettability.

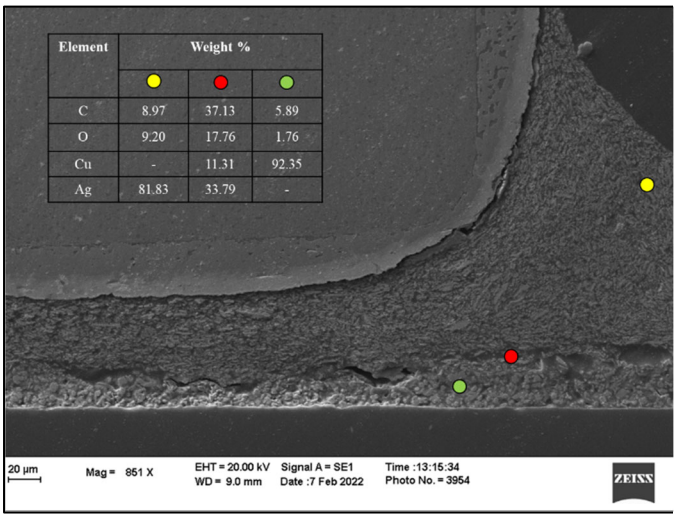

Figure 33: EDX analysis component attachment using ECA

The EDX analysis at the cross-sectional area of the component attached using ECA is shown in Figure 33. The element composition was studied in three locations, focusing on the copper traces, bonding material, and interconnection between the two layers. The green dot indicates the location of element composition on copper traces. It can be seen that the oxygen level in the material is negligible, with copper making up the majority of the contribution, given the fact that copper has not been oxidized. The red dot represents the interconnectedness of materials, and it is made up of copper and silver, with silver coming from the ECA.

B. Attachment using LTS1(SnBiAg)

The electrical measurements of discrete components attached to LTS1 are shown in Figure 34 - Figure 36. The modules were tested at different frequencies to see how frequency affected performance. The calculated values are within a reasonable range.

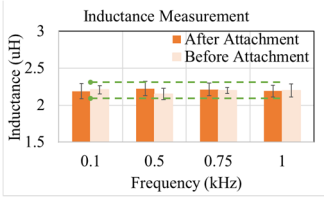

Figure 34: Measurement of the inductor at various frequencies in comparison to rated value

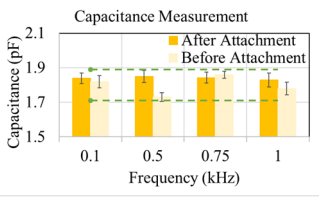

Figure 35: Measurement of the capacitor at various frequencies in comparison to rated value

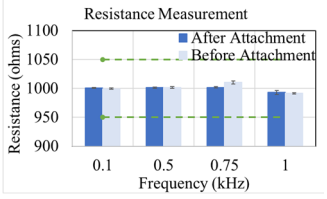

Figure 36: Measurement of the resistor at various frequencies in comparison to the rated value

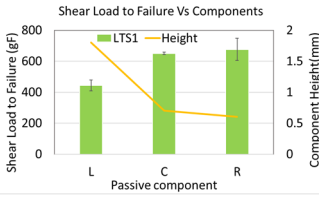

Figure 37: Effect Of various component height attachment with LTS1 on Shear Load to Failure value

It can be observed that the measurements after component attachment using LTS1 material are quite similar to the ones before attachment. Data indicates that there are no additional losses and that the connection bond with the printed copper is stable. Shear test results for various components are shown in **Figure 37**. The data agree with the ECA shear strength values when considering the component height. The interconnect has a higher strength than the ECA attachment.

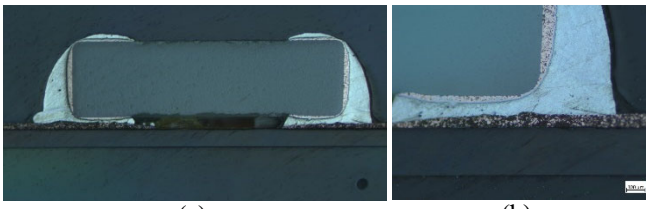

(a) (b)

Figure 38: Cross sectional optical image components attachment using LTS1

The optical image of the component mounted via LTS1 is shown in Figure 38. The cross-sectional image shows the copper and LTS1 bond, with the LTS1 material having reflowed appropriately with no voids. Figure 38 shows that the bonding substance has created a suitable fillet, suggesting acceptable wettability. Figure 39 shows the EDX analysis of the component mounted using LTS1 at the cross-sectional region. The element composition was studied at three separate levels, as previously explained in the ECA section. The analysis has been consistent across all binding materials. It can be seen that the oxygen level in the material is negligible. The connectivity point has a mix of copper and LTS1 components as needed. The yellow dot closely resembles solder substances. The solder region has grain patterns produced, ensuring appropriate reflow.

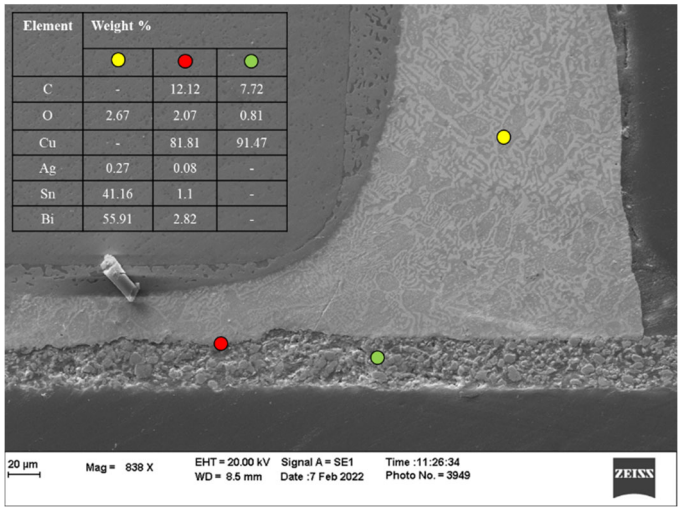

Figure 39: EDX analysis for component using LTS1

C. Attachment using LTS2 (SnIn)

Figure 40-Figure 42 show RLC discrete component measurements after attaching using LTS2 (SnIn) material. The coupons were tested at various frequencies to see how frequency affected performance. The calculated values fall within an acceptable range. It can be observed that the post

component attachment value is somewhat higher in this case than the individual components evaluated before attachment.

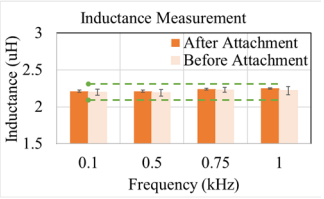

Figure 40: Measurement of the inductor at various frequencies in comparison to rated value

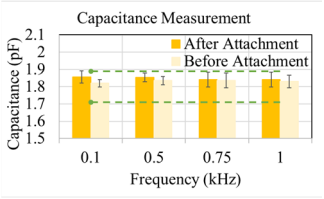

Figure 41: Measurement of the capacitor at various frequencies in comparison to rated value

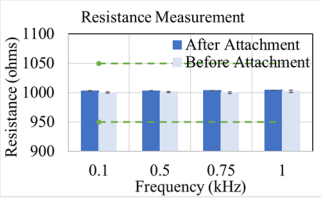

Figure 42: Measurement of the resistor at various frequencies in comparison to the rated value

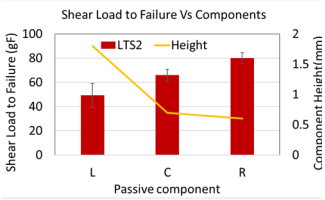

Figure 43: Effect of various component height attachment with LTS2 on Shear Load to Failure value

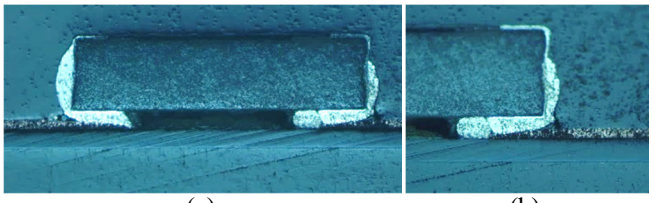

(a) (b)

Figure 44: Cross-section optical image of components attachment using LTS2

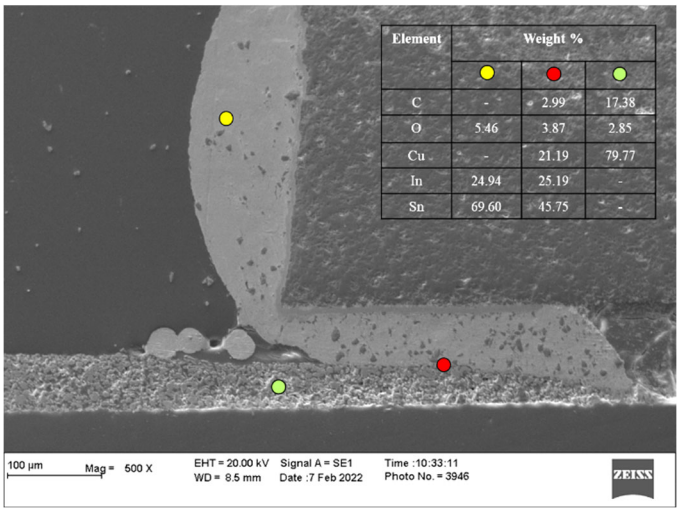

Figure 45: EDX analysis of attachement using LTS2

Figure 43 depict shear test results for discrete components used. When the mechanical strength of the three binding materials is compared, LTS2 performs the worst. As a result, the SnIn solder does not provide adequate mechanical strength with additive printed copper and established sintering conditions. Figure 44 illustrates the optical image of the component connected with LTS2. The optical image shows that the copper bond with the LTS2 material does not form a good joint. The solder forms a ball rather than a fillet shape, indicating oxidation or a lack of bonding strength. This is connected to the mechanical strength value, which is significantly lower than the other two binding material connections. Figure 45 illustrates the EDX analysis of the component mounted using LTS2 at the cross-sectional region. The interconnection location is often made up of copper and LTS2 elements. The yellow dot closely resembles solder material. It can also be shown that the oxygen concentration in the LTS2 attachment is greater than in the LTS1 analysis, indicating that oxidation may be the reason for insufficient bonding.

D. Comparison of ECA, LTS1 and LTS2

The components were tested at 1kHz frequency for comparison. Figure 46 - Figure 48 compare the electrical performance of several discrete components in respect to various binding materials. For comparison, the components were tested at 1kHz. The main finding is that the components are well within the tolerance range specified by the manufacturer. The inductors tend to read almost the same value with ECA and LTS1 attachments, however, there is considerable fluctuation with LTS2 attachment compared to prior attachment readings. Similarly, with prior attachment measurements, the ECA and LTS1 materials exhibit lesser variation than the LTS2 material. In comparison to capacitors and inductors, resistors have a distinct tendency. The LTS1 and LTS2 materials have the least variance with resistors.

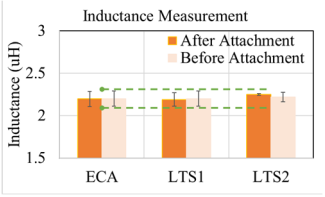

Figure 46: Electrical performance comparison of inductor attachment vs binding material

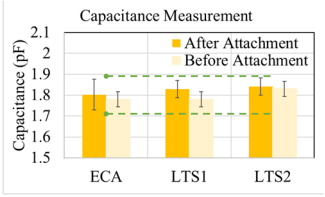

Figure 47: Electrical performance comparison of capacitor attachment vs binding material

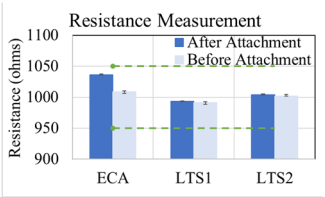

Figure 48: Electrical performance comparison of resistor attachment vs binding material

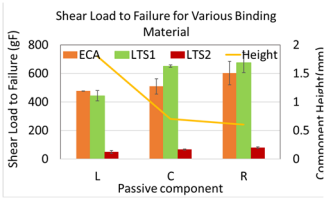

Figure 49: Mechanical performance comparison of discrete component attachment for binding material

According to Figure 49, mechanical strength tends to decrease with increasing component height. The LTS1 material has the greatest strength, followed by ECA and LTS2. The SEM/EDX research also revealed that the LTS1 joint exhibited the best mechanical and electrical performance out of the interconnect system analyzed in this study.

FLEX TO INSTALL - FOLDING RELIABILITY:

The samples were evaluated in their folded state on a 25mm and 50mm diameter curve. In all three scenarios, the LED sustains mechanical failure with the two fold-diameters. The LEDs were checked for functionality by applying 2 volts across the pads.

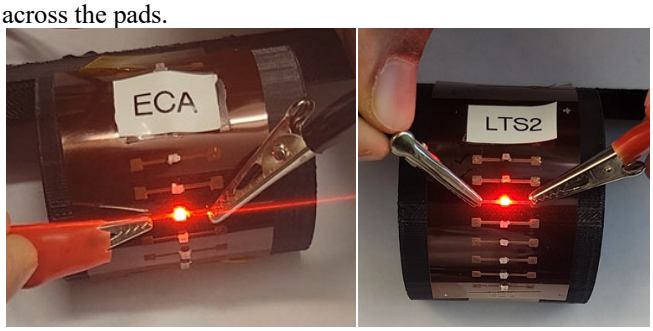

(a) (b)

Figure 50: Test sample of a coupon on 25mm diameter fold

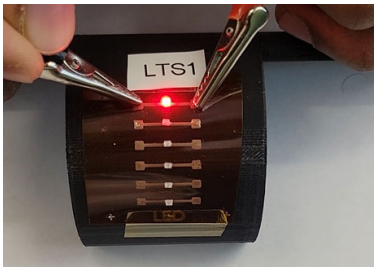

Figure 51: Test sample of a coupon on 50mm diameter fold

Figure 50-Figure 51, it can be observed that the circuits are functional. The supply voltage required to turn on the LEDs was the same as when tested in the flat state, demonstrating that the binding materials are strong enough to withstand shear stresses. The electrical parameters did not change because the circuit lit up at the same voltage.

AMPLIFICATION APPLICATIONS

Test results from design-1 serve as the foundation for the printing parameters. The print parameters are finalized considering the effect of print speed and ink pressure on the trace profile later relating it to mechanical and electrical properties. The circuit is designed for an amplified inverting circuit.

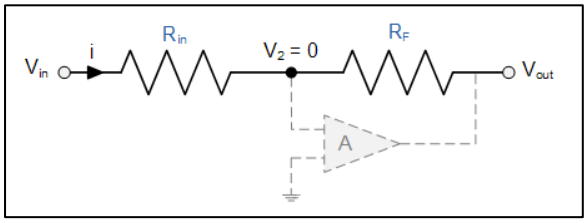

Figure 52: Schematic for the Inverting Amplifier

The circuit was designed with a certain gain in consideration. Rf = 10kOhms and Rin = 4.7kOhms were utilized as resistors in the circuit shown in Figure 52. The gain calculation for it is as follows:

$$\text{Gain} = -\frac{Rf}{Rin} \quad (1)$$

The gain of the circuit is 2.13 for the components utilized in it. Figure 53 shows the actual printed flexible op-amp circuit. The figure depicts the notation of the connections used to power the circuit. Assembly is demonstrated on a flexible substrate to assess viability for FHE application with ECA attachment.

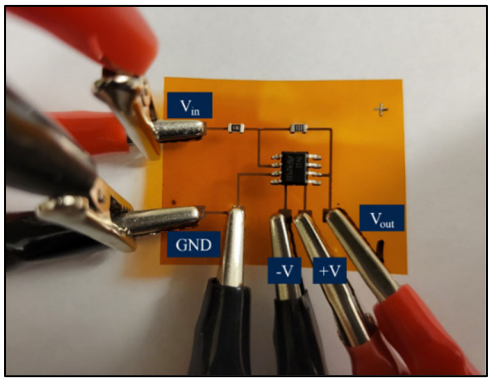

Figure 53: Printed flexible Inverting Op-Amp circuit

The components utilized are 0805 sizes, which are in the middle of the size range for components used in industrial applications. A sinusoidal wave from a wave generator with a 50ohm load was fed into the input. An oscilloscope was used to record the input and output signals. The circuit was been powered with a ±15V DC supply as recommended for the Op-Amp. After the samples were tested, there was little wear of the pads due to the crocodile clip, and we were able to retest them, but for future analysis, we want to utilize conductive epoxy to attach wires for stable connections.

A. Attachment using ECA

Figure 54 depicts a performance comparison of the Op-Amp circuit at 3kHz. The simulated and the oscilloscope data from printed circuits were compared. It can be shown that the simulated data and the actual data obtained nearly match, implying that component attachment by ECA is feasible and might be investigated for further application in flexible electronics. There is some noise in the sine curve's partial region, which is significant during the start of the upsweep or down sweep. To investigate further we have tested the test coupon at 10kHz as well.

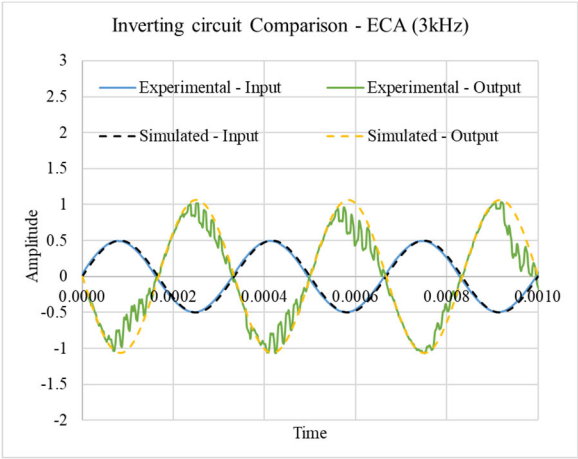

Figure 54: Performance comparison of the Amplified inverting circuit at 3kHz

B. Attachment using LTS1 (SnBiAg)

Figure 55 shows the performance comparison of the Op-Amp circuit at 3kHz for circuit attachment using LTS1. The curves match when the simulated and oscilloscope data from printed circuits were compared. In this case, the experimental value has shifted slightly in the y-direction. This circuit has less noise than the ECA attached circuit.

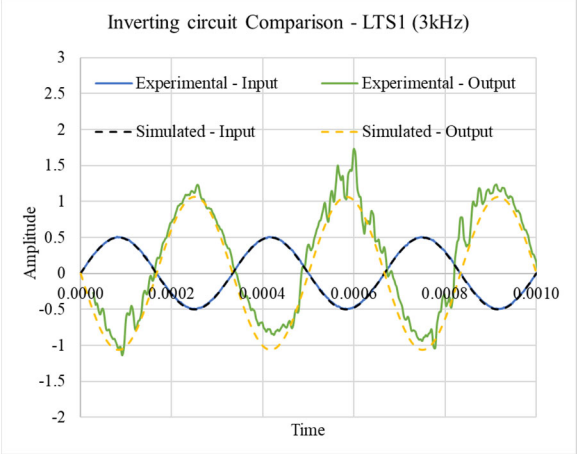

Figure 55: Performance comparison of the Amplified inverting circuit at 3kHz

C. Attachment using LTS2 (SnIn)

Figure 56 compares the performance of the Op-Amp circuit at 3kHz for circuit attachment using LTS2. The curves match when the simulated and oscilloscope data from printed circuits were compared. In this situation, the experimental value has also shifted somewhat in the y-direction. In comparison to the other two circuits, this one has the least amount of noise.

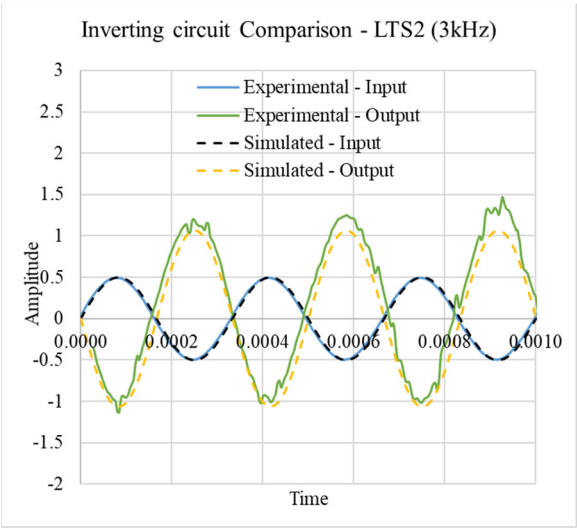

Figure 56: Performance comparison of the Amplified inverting circuit at 3kHz

II. SUMMARY AND CONCLUSIONS

This paper studied various sintering conditions for additively printed copper on the direct-write platform. Factors studied include preheat, stage speed, and flash energy. The effect of preheating has been studied to assess the ability to mitigate the popcorning of printed metallization. The EDX study was performed to demonstrate that preheating is advantageous. These test results from test vehicle-1 were utilized to investigate the impact of additional curing processes in real-world applications. Depending on the application, the test vehicle's two design incorporates component attachments such as resistors, capacitors, inductors, and LEDs. These are some of the most common circuitry components. The direct-write approach for connecting the components has been established. In order to estimate the percentage variation introduced by the additive printing attachment, the components were tested before and after the attachment. The measured values were well within the rated values of the manufacturer. For this study, the lack of understanding about the various binding materials was taken into account, and correct attachment issues were shown. Compared to silver-based ECA and SnIn low-temperature solders, SnBiAg solder provides the greatest performance. The EDX analysis is also used to address the causes of the failure situations. Based on the study of the test vehicle-1, the functionality of the component attachment was further investigated by building an amplified inverting Op-Amp circuitry. The design was initially modeled in software and compared to the system's real performance. Although a 15V DC source supplied the circuit, no degradation in the printed traces was noticed. This also means that the technology may be used for high-power circuits like this one. The performance comparison produces favorable results, indicating that the process development was carried out in order to develop functioning circuitry. All three binding materials give a fundamental knowledge of the material in high-frequency applications.

ACKNOWLEDGMENTS

The project was sponsored by the NextFlex Manufacturing Institute under PC6.4 Project titled – ECAs Magnetic Oriented Anisotropic Conductive Adhesives and Low-temperature Solders for FHE in Harsh Environments. This material is based, in part, on research sponsored by Air Force Research Laboratory under agreement number FA8650-20-2-5506, as conducted through the flexible hybrid electronics manufacturing innovation institute, NextFlex. The U.S. Government is authorized to reproduce and distribute reprints for Governmental purposes notwithstanding any copyright notation thereon. The views and conclusions contained herein are those of the authors and should not be interpreted as necessarily representing the official policies or endorsements, either expressed or implied, of Air Force Research Laboratory or the U.S. Government.

REFERENCES

[1] Niittynen, J., Kiilunen, J., Putaala, J., Pekkanen, V., Mäntysalo, M., Jantunen, H., & Lupo, D. (2012). Reliability of ICA attachment of SMDs on inkjet-printed substrates. *Microelectronics Reliability*, *52*(11), 2709-2715

[2] Molesa, S. E. (2006). Ultra-low-cost printed electronics.

[3] Hu, A., Guo, J. Y., Alarifi, H., Patane, G., Zhou, Y., Compagnini, G., & Xu, C. X. (2010). Low temperature sintering of Ag nanoparticles for flexible electronics packaging. *Applied Physics Letters*, *97*(15), 153117.

[4] Cui, Q., Gao, F., Mukherjee, S., & Gu, Z. (2009). Joining and interconnect formation of nanowires and

carbon nanotubes for nanoelectronics and nanosystems. *Small*, *5*(11), 1246-1257.

[5] Lu, C. A., Lin, P., Lin, H. C., & Wang, S. F. (2007). Effects of silver oxide addition on the electrical resistivity and microstructure of low-temperature-curing metallo-organic decomposition silver pastes. *Japanese Journal of Applied Physics*, *46*(7R), 4179.

[6] Mir, I., & Kumar, D. (2008). Recent advances in isotropic conductive adhesives for electronics packaging applications. *International journal of adhesion and adhesives*, *28*(7), 362-371.

[7] Lau, J. H., Wong, C. P., Lee, N. C., & Lee, S. W. R. (2003). *Electronics manufacturing: with lead-free, halogen-free, and conductive-adhesive materials*. McGraw-Hill Education.

[8] Guan, Y., Chen, X., Li, F., & Gao, H. (2010). Study on the curing process and shearing tests of die attachment by Ag-epoxy electrically conductive adhesive. *International journal of adhesion and adhesives*, *30*(2), 80-88.

[9] Sahasrabudhe, S., Mokler, S., Renavikar, M., Sane, S., Byrd, K., Brigham, E., ... & Parupalli, S. (2018, May). Low Temperature Solder-A Breakthrough Technology for Surface Mounted Devices. In *2018 IEEE 68th Electronic Components and Technology Conference (ECTC)* (pp. 1455-1464). IEEE.

[10] Lall, P., Narangaparambil, J., Schulze, K., & Miller, S. (2021, October). Printed Flexible LC Filter Using Additive Micro-Dispensing With Silver Conductive Paste and ECA for Component Attachment. In *International Electronic Packaging Technical Conference and Exhibition* (Vol. 85505, p. V001T03A006). American Society of Mechanical Engineers.

[11] Lall, P., Narangaparambil, J., Leever, B., & Miller, S. (2019, May). Effect of Sintering Temperature on the Fatigue Life of Additively Printed Electronics During Cyclic Bending. In 2019 18th IEEE Intersociety Conference on Thermal and Thermomechanical Phenomena in Electronic Systems (ITherm) (pp. 189-197). IEEE.

[12] Harkai, E., Balogh, B., & Latos, I. (2010, May). Effects of test conditions on shear strength of surface mount solder joints. In 33rd International Spring Seminar on Electronics Technology, ISSE 2010 (pp. 208-211). IEEE.

[13] Lall, P., Narangaparambil, J., Schulze, K., & Hill, C. (2021, June). Process Recipes for Additively Printed Copper-Ink Flexible Circuits using Direct Write Methods. In 2021 20th IEEE Intersociety Conference on Thermal and Thermomechanical Phenomena in Electronic Systems (iTherm) (pp. 1061-1072). IEEE.